Ba $6png$, $J=3$ and $J=5$ autoionizing states

S. M. Jaffe,* R. Kachru, H. B. van Linden van den Heuvell,† and T. F. Gallagher‡
Molecular Physics Department, SRI International, 333 Ravenswood Avenue, Menlo Park, California 94025
(Received 14 February 1985)

We report the energies and autoionization rates of the Ba $6png$, $J=3$ and $J=5$ states which we have obtained by multistep laser spectroscopy. The observed $6png$ states have small quantum defects (0.03), and widths of 0.05 n^{-3}. The $J=3$ and $J=5$ series converging to the Ba^+ $6p_{1/2}$ limit are degenerate while the two $J=3$ and two $J=5$ series converging to the Ba^+ $6p_{3/2}$ limit are easily distinguished. The splittings are in good agreement with the electric quadrupole splittings calculated by assuming nonpenetrating ng orbitals. The autoionization rates are also in accord with estimates assuming nonpenetrating orbitals.

I. INTRODUCTION

Autoionizing Rydberg states in which one electron is in an orbit of high angular momentum around an excited ionic core are interesting from both practical and fundamental points of view. For example, the multiplicity of the high angular momentum states makes them very important in dielectronic recombination in spite of their relatively low autoionization rates.[1] On the other hand, these atoms are interesting from a fundamental point of view because, to a good approximation, one of the two valence electrons is always the inner electron and one is always the outer electron. Thus in these states autoionization occurs through a long-range interaction, not by penetration of the ion core by the outer electron. The properties of such atoms should therefore be a good test of atomic-structure calculations.

As such atoms are optically inaccessible from the ground state with a single photon, little attention has been paid to them until the advent of multistep laser excitation techniques which have allowed the selective population of high angular momentum states. This was first done by Cooke *et al.*[2] who used a Stark switching technique to populate bound Sr $5snl$ states and were thus able to excite specific $5pnl$ autoionizing states for $l<7$, where n and l are the principal and orbital angular momentum quantum numbers. Here we report the study of the Ba $6png$, $J=3$ and 5 states using a zero-field four-step laser excitation-cascade approach which allows us to preserve J as a good quantum number.

We briefly describe the method and present our results which consist of the energies and widths of the $6png$ states and the perturbed spectra produced by the interaction of the series converging to the Ba^+ $6p_{3/2}$ and $6p_{1/2}$ limits. We then show that the splittings of the levels converging to the Ba^+ $6p_{3/2}$ limit are consistent with an electric quadrupole interaction; this allows us to identify the appropriate coupling scheme of the atom and assign the levels. Finally, we provide a quantum-defect-theory simulation of our results for the $J=5$ states to tie together the different manifestations of the $6p_{3/2}ng_k-6p_{1/2}ng_{9/2}$ interseries interaction and condense the observations into a small number of physically significant parameters.

II. EXPERIMENTAL APPROACH

The general approach we have used is multistep laser excitation of Ba atoms in an effusive beam to autoionizing states followed by the detection of ions from the decay of the autoionizing atoms.

The laser excitation scheme is shown in Fig. 1. A 5535-Å pulsed tunable dye laser excites the Ba atoms to the $6s6p\ ^1P_1$ state from which 5% decay to the metastable $6s5d\ ^1D_2$ state. About 100 ns later a second dye laser at 6482 Å excites the atoms in the $6s5d\ ^1D_2$ state to the $5d6p\ ^1F_3$ state, and 5 ns later a third dye laser excites these atoms to the $6sng\ ^1G_4$ state. Finally, the fourth laser, which is scanned in wavelength, excites the bound Ba $6sng$ atoms to the autoionizing $6png$ state. The wavelength of the fourth laser is very near one of the two Ba^+ resonance lines at 4555 or 4935 Å, and the excitation to the $6png$ state is essentially the resonance line excitation of Ba^+ with a spectator ng electron.[2] It therefore has an oscillator strength of one spread over a few wave numbers. As this is stronger by orders of magnitude than the excitation to the underlying continua, there is no observable interference between the direct continuum excitation and the excitation to the discrete autoionizing state. This corresponds to the Fano q parameter equal to infinity,[3] in

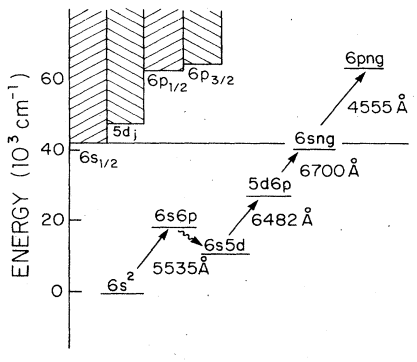

FIG. 1. $6png$ energy levels and the levels used in the excitation. Laser excitation steps are shown as straight arrows. The cascade is shown as a wavy arrow.

which case the observed spectrum is a Lorentzian yielding immediately the position and width of the autoionizing state.

As shown in Fig. 1 our excitation method includes the cascade $6s\,6p\,{}^1P_1$—$6s\,5d\,{}^1D_2$ transition which in principle diminishes the J selectively in the excitation of the autoionizing $6png$ states. To assess the severity of the diminution in selectivity we have calculated the final states produced with our two polarization schemes, all four lasers polarized linearly and parallel, and all four lasers polarized circularly in the same sense. For the lasers all circularly polarized the $J=5$ states are by far the most prominent just as if five circularly polarized lasers were used.[4,5] Similarly, for linear polarization predominantly $J=3$ and 5 states are observed as would be strictly the case for five linearly polarized lasers. Thus in spite of the cascade and the fact that the alignment of the odd isotopes, of 18% abundance, is largely destroyed by hyperfine structure in the $6s\,6p\,{}^1P_1$ state,[6] the J selectivity is quite satisfactory.

The apparatus used in these experiments has been described elsewhere,[7] so our description here is brief. The four dye lasers are of both the Hansch[8] and Littman[9] designs with the following typical parameters; 100-μJ pulse energy, 5-ns pulse duration, and 0.6-cm^1 linewidth. The dye lasers are pumped by harmonics of a Nd:YAG laser operating at 10 Hz. As noted above the second dye-laser pulse is delayed by 100 ns from the first, and the third and fourth dye-laser pulses come at 5-ns intervals after the second. To determine the relative wavelength scale of the scanned fourth laser we record the transmission through a 3.54-cm^{-1} free spectral range etalon. To put the wavelength scale on an absolute basis we periodically pump the first laser twice, the second time just before the fourth laser to ensure that there are some Ba $6s\,6p$ atoms present when the fourth laser excites the atoms. In this case the fourth laser can drive the two-step process $6s\,6p \rightarrow 6snd(s) \rightarrow 6pnd(s)$ which occurs at several wavelengths near the Ba$^+$ resonance lines at 4555 and 4935 Å. These features, occurring at the known $6s\,6p$-$6snd(s)$ wavelengths,[10] serve as our absolute wavelength standard.

The atomic beam apparatus is a vacuum vessel 0.5 m in diameter at a pressure of less than 10^{-6} Torr in which an effusive Ba-atom beam from a heated oven passes between a plate and a grid 1 cm apart, where the Ba atoms are excited by the laser beams. About 0.5 μs after the last laser pulse a 500-V pulse is applied to the plate forcing any ions formed by the excitation and subsequent decay of a Ba $6png$ state through the grid to a particle multiplier. The signal from the multiplier is detected with a gated integrator and recorded with an x-y recorder.

III. EXPERIMENTAL RESULTS

Before describing our results in detail it is helpful to present a brief summary.

With circularly polarized light we observed one series converging to the Ba$^+$ $6p_{1/2}$ limit and two series converging to the Ba$^+$ $6p_{3/2}$ limit. These are the three $J=5$ series. With linearly polarized light, which allows the excitation of the $J=3$ states as well, we observed two additional series converging to the Ba$^+$ $6p_{3/2}$ limit. However, the spectra of states converging to the $6p_{1/2}$ limit obtained with linearly and circularly polarized light were nearly indistinguishable. The fact that there is negligible splitting of the $J=3$ and $J=5$ states converging to the $6p_{1/2}$ limit suggests that there is negligible spin-orbit coupling of the outer electron. Based on the small spin-orbit splittings of the bound $6sng$ states[11] this is not unexpected. The presence of substantial splittings between the series converging to the Ba$^+$ $6p_{3/2}$ limit is thus unlikely to be due to a spin-orbit effect, but rather to the electric quadrupole interaction of the ng electron with the $6p_{3/2}$ ion core. This suggests that the most appropriate coupling scheme is one in which the quadrupole interaction

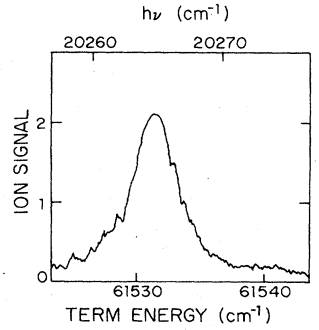

FIG. 2. Ion signal obtained with the first three laser wavelengths set to populate the bound $6s\,12g\,{}^1G_4$ state as the fourth-laser wavelength is scanned across the $6s\,12g\,{}^1G_4$—$6p_{1/2}12g_{9/2}$ transition near 4935 Å. All four lasers are circularly polarized in the same sense.

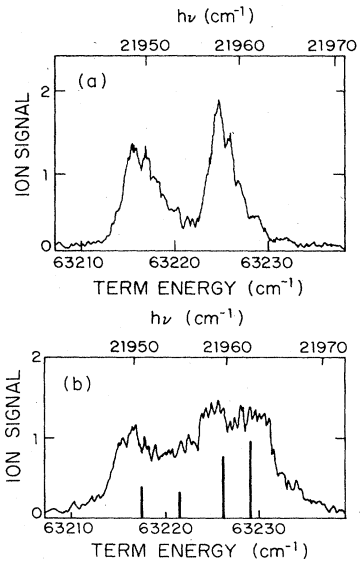

FIG. 3. Ion signal obtained with the first three laser wavelengths set to excite the bound $6s\,12g\,{}^1G_4$ state as the fourth-laser wavelength is scanned across the $6s\,12g\,{}^1G_4$ to $6p_{3/2}12g_k$ transitions near 4555 Å. (a) With all four lasers circularly polarized in the same sense. (b) With all four lasers colinearly polarized. Computed positions and intensities of the $J=3$ and 5 levels are indicated by the vertical bars.

has only diagonal matrix elements. Thus we have used $j_1 l_2$ coupling, where j_1 and l_2 are the total angular momentum of the Ba^+ ion core and the orbital angular momentum of the ng electron. We define their vector sum by $\vec{k}=\vec{j}_1+\vec{l}_2$. The total angular momentum J is defined by $\vec{J}=\vec{k}+\vec{s}_2$, where s_2 is the spin of the ng electron. We thus describe the $6png$ states as $6_{j_1}ng_k$.

Typical examples of our observations with circularly polarized light are shown in Figs. 2 and 3(a) which are scans of the fourth-laser wavelength in the vicinity of 4935 and 4555 Å when the first three lasers populate the $6s\,12g\,^1G_4$ state. From data such as these we easily extract the energies and autoionization widths [full width at half maximum (FWHM)] of these states.

The widths are simply read from the recordings such as Figs. 2 and 3. The energies are determined by adding photon energy of the center of the ion signal peak to the known energies of the $6s\,^1G_4$ states. For $n>8$ we have taken the energies from Camus *et al.*,[11] and we have measured the $6s\,6g\,^1G_4$ and $6s\,7g\,^1G_4$ term energies to be 38 945(1) and 39 765(1) cm^{-1}, respectively.

In Tables I and II we list our results for the $6p_{1/2}ng_{9/2}$ states and $6p_{3/2}ng_k$ $J=5$ states, respectively, with the assignment of the k quantum number derived in Sec. IV. In Tables I and II we have followed the usual convention for the effective quantum number n^* and quantum defect δ. They are defined by the binding energy W relative to the limit in question by the relation

$$W=-1/[2(n^*)^2]=-1/[2(n-\delta)^2]\ , \tag{1}$$

in which the energy is given in atomic units. In Tables I and II we give also the term energies and widths of the $J=5$ states resulting from a quantum-defect-theory fit to our data.[12]

As shown by Tables I and II the quantum defects of the $6png$ states are generally constant. Similarly the widths Γ have an approximate overall n^{-3} dependence, however there is a systematic energy dependence which is brought out by Fig. 4, a plot of the scaled autoionization rate $n^3\Gamma$ versus term energy.

Ignoring the increase in $n^3\Gamma$ which occurs near the $6p_{1/2}$ and $6p_{3/2}$ limits, which is probably an experimental artifact, we can see that $n^3\Gamma$ monotonically increases with energy, and that all the data, perturbations excepted, are reasonably represented by

$$n^3\Gamma=7.4(4)\times10^3+1.08(20)\Delta E\ , \tag{2}$$

where $\Delta E=E-62\,000\ cm^{-1}$, E being the term energy in cm^{-1}, and $n^3\Gamma$ is given in cm^{-1} as is Fig. 4. The average scaled autoionization rate is $7.4\times10^3\ cm^{-1}$, corresponding to an autoionization rate of $\Gamma=0.034n^{-3}$ in atomic units.

When we excite the $6p_{1/2}ng_k$ states with linear polarization we observe in general a broader feature slightly blue shifted from the $J=5$ feature observed with all four lasers circularly polarized. From these observations we conclude that the $J=3$ states lie $0.002n^{-3}$ above the $J=5$ states. The only exception to this is $n=14$ for which we see two different peaks which we can clearly identify as being $J=3$ and 5 states. The $J=3$ feature occurs at 61 742.8 cm^{-1} and has a width of 4.03 cm^{-1} and an effective quantum number of 14.08. Both $J=3$ and 5 features are perturbed from their expected position by interaction with the $6p_{3/2}7g_k$ states. However, the $J=3$ state is perturbed in energy far more than the $J=5$ state indicating a generally stronger interseries interaction

TABLE I. $6p_{1/2}ng_{9/2}$ $J=5$ states observed with circular polarization. The uncertainties in the widths are 15% or 0.5 cm^{-1}, whichever is greater, and the uncertainties in the term energies are half the uncertainties in the widths.

	Observed			Calculated	
n	Term energy (cm^{-1})	Effective quantum number	Width (cm^{-1})	Term energy (cm^{-1})	Width (cm^{-1})
6	59 228.9	5.98	20.38	59 221	30
7	60 049.1	6.99	15.43	60 050	18
8	60 573.8	7.98	14.52	60 573	13
9	60 943.1	9.00	14.42	60 924	18
10	61 195.2	9.98	7.02	61 197	7.5
11	61 385.8	10.98	5.34	61 387	5.3
12	61 531.4	11.98	4.37	61 532	4.2
13	61 644.1	12.97	3.23	61 644	3.8
14	61 736.3	14.00	3.83	61 734	6.2
15	61 808.2	14.99	2.31	61 809	2.3
16	61 866.3	15.97	1.65	61 868	2.5
17	61 916.1	16.98	1.55	61 916	2.2
18	61 957.6	18.00	1.23	61 957	2.0
19	61 992.8	19.01	1.48	61 922	1.5
20	62 021.5	19.98	1.47	62 022	2.2
21	62 047.4	20.99	1.15	62 047	1.8
22	62 069.8	22.00	0.84	62 069	1.5
23	62 088.4	22.97	1.09	62 089	1.2

TABLE II. $6p_{3/2}ng_k$, $J=5$ states observed with circular polarization. The uncertainties in the widths are 15% or 0.5 cm^{-1}, whichever is greater, and the uncertainties in the term energies are half of the uncertainties in the widths.

		Observed			Calculated	
n	k	Term energy (cm^{-1})	Effective quantum number	Width (cm^{-1})	Term energy (cm^{-1})	Width (cm^{-1})
6	11/2	60 942.9	6.00	23.32	60 940	45
	9/2	60 868.5	5.93	13.47	60 862	25
7	11/2	61 747.0	7.00	17.83	61 760	14
		61 716.6	6.95	9.09		
	9/2	61 703.4	6.93	10.29	61 702	14
8	11/2	62 272.5	8.00	15.01	62 272	11
	9/2	62 242.3	7.93	14.71	62 241	12
9	11/2	62 633.1	9.00	12.26		
	9/2	61 612.7	8.93	11.96		
10	11/2	62 889.8	10.00	6.70		
	9/2	62 875.6	9.94	8.64		
11	11/2	63 079.9	11.00	5.09		
	9/2	63 069.0	10.93	5.90		
12	11/2	63 225.1	12.00	5.72		
	9/2	63 216.9	11.93	5.62		
13	11/2	63 338.2	13.00	3.65		
	9/2	63 331.6	12.94	4.29		
14	11/2	63 427.3	14.00	2.75		
	9/2	63 421.6	13.93	3.38		
15	11/2	63 499.2	14.99	2.30		
	9/2	63 494.7	14.92	2.94		
16	11/2	63 557.6	15.98	2.28		
	9/2	63 554.3	15.92	2.37		
17	11/2	63 607.6	17.00	2.38		
	9/2	63 603.5	16.91	2.38		
18	11/2	63 648.7	18.00	2.11		
	9/2	63 646.1	17.93	1.54		
19	11/2	63 683.8	19.01	1.37		
	9/2	63 681.3	18.94	1.37		
20	11/2	63 712.6	19.99	1.13		
	9/2	63 710.5	19.91	1.04		
21	11/2	63 738.6	21.00	1.07		
	9/2	63 736.8	20.93	1.07		
22	11/2	63 760.8	22.01	0.93		
	9/2	63 759.0	21.92	0.96		
23	11/2	63 779.9	23.00	0.69		
	9/2	63 778.4	22.92	0.84		
24	11/2	63 798.1	24.08	0.69		
	9/2	63 797.0	24.01	0.87		
25	11/2	63 811.7	25.00	0.71		
	9/2	63 810.8	24.93	0.71		

for the $J=3$ states.

As mentioned earlier, when we excite the $6p_{3/2}ng_k$ states with linearly polarized lasers we observe two additional states which we assign as $J=3$. An example of this is shown in Fig. 3(b). In Table III we give the positions and widths of the $6p_{3/2}ng_k$ $J=3$ states. As in Table II the k assignments will be justified in Sec. III. It is evident that the widths of the $J=3$ states may not be determined with the same precision as those of the $J=5$ states due to the congestion of the spectra, thus the widths listed in Table III are not as precise as those given in Table II.

The $6p_{3/2}ng_k$ states below the Ba^+ $6p_{1/2}$ limit interact with the $6p_{1/2}ng_k$ states, and if we focus our attention on the $J=5$ states we can see several interesting manifestations of this interseries interaction. First, there are some small perturbations in the energies of the $6p_{1/2}ng_{9/2}$ levels at $n=9$ and 14. Specifically these two levels are both shifted up in energy by $0.02n^{-3}$. The fact that they are shifted up implies that they interact with the $6p_{3/2}ng_{9/2}$ states more strongly than with the $6p_{3/2}ng_{11/2}$ states, for interactions with the latter states would tend to lower the energies of these two $6p_{1/2}ng_{9/2}$ states. This is in accord with our expectations if a quadrupole coupling is the most important interseries interaction. The quadrupole matrix

TABLE III. $6p_{3/2}ng_k$, $J=3$ states observed with linear polarization. The uncertainties in the widths are 30% or 0.5 cm^{-1}, whichever is greater, and the uncertainties in the term energies are half the uncertainties in the widths.

n	k	Term energy (cm^{-1})	Width (cm^{-1})
6	5/2	60 979.2	23.76
	7/2	60 889.1	14.03
7	5/2	61 771.1	16.56
	7/2	61 714.8	10.96
8	5/2	62 288.6	13.79
	7/2	62 253.9	12.04
9	5/2	62 644.6	10.60
	7/2	62 621.7	9.09
10	5/2	62 898.1	6.65
	7/2	62 881.4	5.01
11	5/2	63 085.7	4.83
	7/2	63 073.9	3.93
12	5/2	63 229.2	3.67
	7/2	63 220.0	3.48
13	5/2	63 341.7	3.69
14	5/2	63 429.9	1.97
15	5/2	63 501.5	2.13
16	5/2	63 560.8	1.60
17	5/2	63 609.4	1.42
18	5/2	63 650.9	1.29

element connecting the $6p_{1/2}ng_{9/2}$ states to the $6p_{3/2}ng_{11/2}$ states vanishes, but the matrix element connecting $6p_{1/2}ng_{9/2}$ to the $6p_{3/2}ng_{9/2}$ states does not.[5] The second manifestation of the interaction is the fact that the autoionization rates of the $6p_{1/2}9g_{9/2}$ and $6p_{1/2}14g_{9/2}$ states are substantially higher than would be expected for an n^{-3} scaling of the autoionization rates. This is brought out clearly by Fig. 4, a plot of the scaled autoionization rate $n^3\Gamma$ as a function of term energy. The fact that the $6p_{1/2}9g_{9/2}$ and $6p_{1/2}14g_{9/2}$ states depart from the n^{-3} dependence of Γ is quite apparent. Correspondingly, the $6p_{3/2}6g_{9/2}$ and $6p_{3/2}7g_{9/2}$ states are noticeably depressed in autoionization rate, presumably from having lost some of their rates to the $6p_{1/2}9g_{9/2}$ and

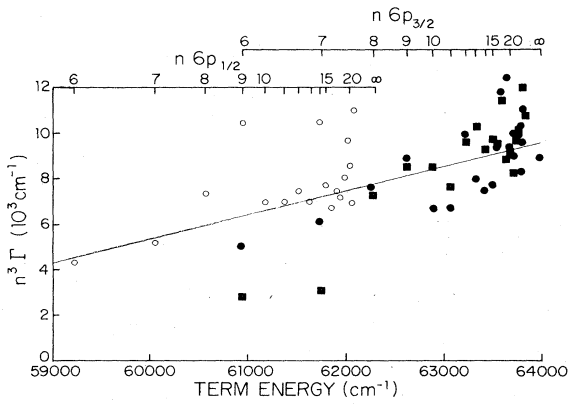

FIG. 4. A plot of the scaled autoionization width $n^3\Gamma$ vs binding energy for $J=5$ states $6p_{1/2}ng_{9.2}$ (○), $6p_{3/2}ng_{9/2}$ (■), $6p_{3/2}ng_{11/2}$ (●).

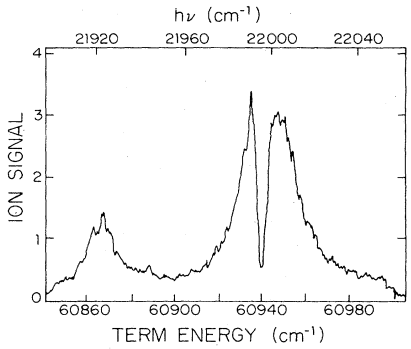

FIG. 5. A scan of the fourth laser across the $6s\,6g\,{}^1G_4-6p_{3/2}6g_k$ transitions at 4555 Å. As shown, the $6p_{3/2}6g_{11/2}$ state, centered at 60 943 cm^{-1}, is degenerate with the $6p_{1/2}9g_{9/2}$ state which produces the hole in the center. All lasers are circularly polarized in the same sense.

$6p_{1/2}14g_{9/2}$ states. Again the interaction is between the $k=\frac{9}{2}$ states.

The final and most dramatic manifestation of the interseries interaction is in the appearance of the excitation spectra of the $6p_{3/2}ng_k$ states. An example of this is

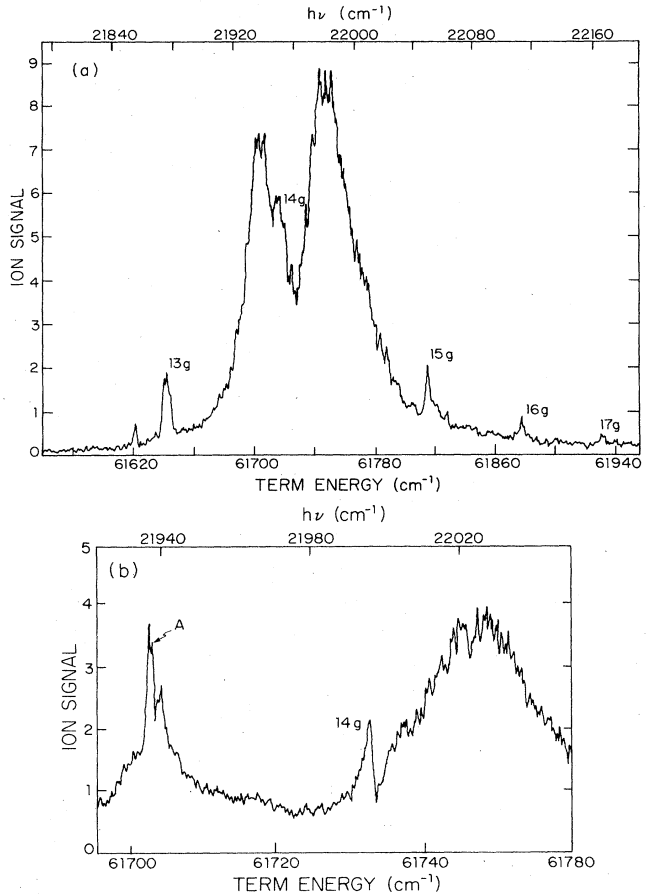

FIG. 6. A scan of the fourth laser across the $6s\,7g\,{}^1G_4-6p_{3/2}7g_k$ transitions at 4555 Å. The small features correspond to the $6p_{1/2}ng_{9/2}$ series as noted. All lasers are circularly polarized in the same sense. (a) Broad scan which is saturated at the center. (b) Lower-laser-power linear scan of the central region. *A* is a two-photon coincidence at 21 938.1 cm^{-1}.

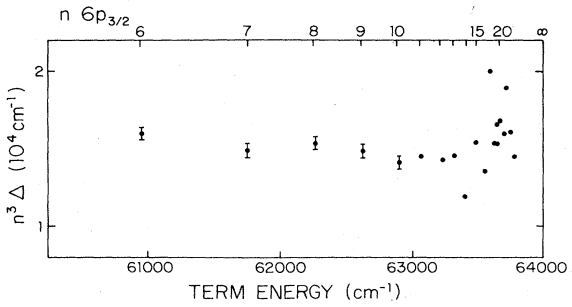

FIG. 7. Plot of the reduced splitting n^3 of the $6p_{3/2}ng_k$ $J=5$ states vs term energy.

shown in Fig. 5, the scan of the fourth laser across the $6p_{3/2}6g_k$ states. The $6p_{1/2}9g_{9/2}$ state is degenerate with the $6p_{3/2}6g_{11/2}$ state, and this is manifested as the hole in the center of the latter state. Similarly, Fig. 6, a scan of the fourth laser across the $6p_{3/2}7g_k$ states, reveals the sharp interferencelike structures at the locations of the $6p_{1/2}ng_{9/2}$ states for $n=12$–17. In recording Figs. 6(a) and 7 we have used a high laser power to enhance the wings of the $6p_{3/2}ng_k$ signals. Thus at the center of $6p_{3/2}ng_k$ state the signal is saturated with the result that it appears broadened. This phenomenon, frequently termed depletion broadening, is described in detail by Cooke *et al.*[13] Figure 6(b) is a higher-resolution scan of the central portion of Fig. 6(a) at a laser power a factor of 7 lower. In this case the observed a signal is linear in the laser power and shows the feature due to the $6p_{1/2}14g_{9/2}$ state more clearly. It also shows at 61 716 cm^{-1} the anomalous feature of Table II. As it does not fit into either $J=5$ series and varies in strength with the tuning of the third laser, we are inclined to interpret this feature as arising from excitation from something other than the $^1G_4$ state with the final state not being $J=5$. The possibility of such an occurrence is the price for using the cascade approach. We note that in both Figs. 5 and 6 the observed spectrum is not due to an interference in the transition amplitudes, but is due to structure in the autoionizing state itself. An experimental indication of this is the observation that the $6sng$-$6p_{1/2}ng_{9/2}$ spectra exhibit simple Lorentzian peaks. Structures such as those of Figs. 5 and 6 have been observed previously[7,14] and explained using quantum-defect theory by Gounand *et al.*[7] and Cooke and Cromer.[12] The interaction of a series of relatively narrow levels with a degenerate broad autoionizing level has also been treated as the interaction of discrete states with a continuum of finite bandwidth by Connerade,[15] and the connection between this point of view and a more rigorous treatment has been shown by Cooke and Cromer.[12] As they point out, if we are exciting the broad resonance, which is the case in Figs. 5 and 6, then the series of narrow levels appears as a series of Beutler-Fano profiles whose q values change from $-\infty$ to $+\infty$ as we go across the broad resonance. This can be seen in Figs. 5 and 6. In Fig. 5 we see the narrow $6p_{1/2}9g_{9/2}$ state in the center of the $6p_{3/2}ng_{9/2}$ state as a $q=0$ profile.

If we examine Fig. 6 carefully we see that the q of the $6p_{1/2}17g_{9/2}$ feature is large in magnitude. The q of the $6p_{1/2}16g_{9/2}$ profile is also large in magnitude and appears to be positive in sign. The q of the $6p_{1/2}15g_{9/2}$ feature is smaller and definitely positive in sign. The q of the $6p_{1/2}14g_{9/2}$ feature is small and negative, and the q of the $6p_{1/2}13g_{9/2}$ feature is large and negative. Thus the q changes sign as we pass through the broad $6p_{3/2}7g_k$ states.

Both the autoionization rates and the splittings of the $6p_{3/2}ng_k$ states depend upon the small r part of the wave functions. The splittings, Δ, of the $6p_{3/2}ng_{9/2}$ and $6p_{3/2}ng_{11/2}$ states only depend upon the $6png$ wave functions and have an n^{-3} dependence as shown by Fig. 7, a plot of $n^3\Delta$ for the $J=5$ states. On the other hand, the scaled autoionization rates $n^3\Gamma$, which depend on both $6png$ and continuum wave functions, increase, which is the opposite of what would be expected for hydrogenic continuum wave functions. This suggests that there is a small continuum phase shift which plays an important role.

IV. ESTIMATES OF SPLITTINGS AND AUTOIONIZATION RATES

In a $6png$ state the ng electron is classically excluded from orbital radii less than $20a_0$ by the centrifugal potential. Here a_0 is the atomic unit of length 0.53 Å. As this is much greater than the orbital radius of the $6p$ electrons (the classical outer turning point is $8a_0$) it is a good approximation to assume that the ng electron is always the outer electron and that the $6p$ electron is always the inner electron. In this approximation the outer ng electron is completely screened from the doubly charged Ba^{++} core by the inner $6p$ electron and sees a purely Coulomb potential from a singly charged ion core. The total $6png$ wave function can then be written as a product of a Coulomb wave function for the inner $6p$ electron and a hydrogenic wave function for the outer ng electron. This simple form results from taking only the first term in a multipole expansion of the Coulomb interaction of the inner and outer electrons.[16] The first term provides the complete screening. Evaluating the higher-order terms gives the k splittings and autoionization rates.

Let us begin by calculating the splittings of the $6p_{3/2}ng_k$ states, as these provide the assignments of Tables II and III. As we have already mentioned, we interpret the splitting of the $6p_{3/2}ng_k$ levels as arising from a quadrupole splitting rather than from a spin-orbit splitting. The quadrupole matrix elements are diagonal in k and J, thus the quadrupole energies W_Q may be written to an excellent approximation as

$$W_Q=(p_{3/2}g_kJ\,|\,\bar{C}_1^{(2)}\cdot\bar{C}_2^{(2)}\,|\,p_{3/2}g_kJ)\langle r_{6p}^2\rangle\langle r_{ng}^{-3}\rangle\ . \tag{3}$$

Here $\bar{C}_1$ and $\bar{C}_2$ are the spherical harmonic vector operators,[5] $\langle r_{6p}^2\rangle=\langle 6p\,|\,r^2\,|\,6p\rangle=30.44a_0^2$ is obtained from a Numerov integration of a Coulomb wave function, and the hydrogenic value for $\langle r_{ng}^{-3}\rangle=\langle ng\,|\,r^{-3}\,|\,ng\rangle$ is $(90n^3)^{-1}$.[16] The angular parts of Eq. (8) are evaluated using the methods of Edmonds.[5] Combining these factors gives the quadrupole energies of the Ba $6p_{3/2}ng_k$ states listed in Table IV. The calculated quadrupole splittings closely reproduce the observed $6p_{3/2}ng_k$ spectra as shown by Fig. 3(b), in which we show the calculated intensities

TABLE IV. Calculated quadrupole energies, splittings and relative intensities of the $6p_{3/2}ng_k$ states and observed splittings and intensities.

State	W_Q	Calculated Relative intensity	Calculated Splitting	Observed Splitting	Observed Relative intensity
$6p_{3/2}ng_{11/2}$, $J=5$	$+0.0246n^{-3}$	0.076			1.0
			$0.0675n^{-3}$	$0.07n^{-3}$	
$6p_{3/2}ng_{9/2}$, $J=5$	$-0.0429n^{-3}$	0.34			0.6
$6p_{3/2}ng_{7/2}$, $J=3$	$-0.0188n^{-3}$	0.31			0.6
			$0.0671n^{-3}$	$0.07n^{-3}$	
$6p_{3/2}ng_{5/2}$, $J=3$	$+0.0483n^{-3}$	1.00			1.0

and positions for the $6p_{3/2}12g_k$ $J=3$ and 5 states. Since we are unable to calculate the quantum defect of the $6png$ state we have assumed that the quantum defect of the unsplit $6p_{3/2}ng_k$ states is 0.018. As shown by Fig. 3(b) and Tables III and V the agreement in the splittings is really quite good although the agreement in the intensities is only qualitative, i.e., the correct $J=3$ and $J=5$ lines are stronger but not by the proper amount. These calculations are the basis of the assignments of Tables II and III.

We also note that since the quadrupole matrix elements are diagonal in k, we expect a strong quadrupole interaction between the $6p_{1/2}ng_{9/2}$ and $6p_{3/2}ng_{9/2}$ series. This is mostly true. As shown by Tables I and II and Fig. 4 the $6p_{3/2}ng_{9/2}$ states share their autoionization rates with the $6p_{1/2}ng_{9/2}$ states. On the other hand, it is clear that there is some interaction between the $6p_{1/2}ng_{9/2}$ and $6p_{3/2}ng_{11/2}$ series, for if there were not, the $q=0$ feature in the $6p_{3/2}ng_{11/2}$ feature of Fig. 5 would not appear. This may be a reflection of the fact that coupling is not pure $\bar{k}=\bar{j}_1+\bar{l}_2$ due to spin-orbit effects, or it may be a manifestation of a coupling this simple model does not include.

We may use this model to compute that autoionization rate of a $6png$ state by evaluating the matrix elements connecting the $6png$ state to the degenerate continua. The autoionization width (FWHM) of state i to continuum j is given by[3]

$$\Gamma_{ij}=2\pi V_{ij}^2 , \tag{4}$$

where V_{ij} is the coupling matrix element between the discrete $6png$ state and a continuum wave function normalized per unit energy. The total autoionization width is given by[3]

$$\Gamma_i=\sum_j \Gamma_{ij} . \tag{5}$$

TABLE V. $J=5$ quantum-defect-theory channels.

Channel number	Designation
1	$6p_{1/2}ng_{9/2}$
2	$6p_{3/2}ng_{9/2}$
3	$6p_{3/2}ng_{11/2}$
4	continuum
5	continuum
6	continuum

Since the autoionization rates of all the $6png$ states follow the same scaling it is reasonable to ignore the spins of the electrons and estimate the autoionization rate of a spinless $6png$ atom. The autoionization of $6png$ to $6s\epsilon h$ is typical having the V_{ij} matrix element

$$V_{ij}=\langle 6png \mid \bar{C}^{(1)}_1\cdot\bar{C}^{(1)}_2 \mid 6s\epsilon h\rangle r_{6p6s}r^{-2}_{ng\epsilon h} . \tag{6}$$

The angular part of Eq. (6) is evaluated using the methods of Edmonds.[5] The Ba^+ r_{6p6s} and r_{6p5d} matrix elements, $4.33a_0$ and $2.59a_0$, respectively, are derived from the work of Lindgard and Nielsen,[18] and the $r^{-2}_{ng\epsilon h}$ matrix elements are evaluated by Numerov integration of hydrogen wave functions. Inspection of the radial integrals indicates that $r^{-2}_{ng\epsilon h}$ is substantially larger than $r^{-2}_{ng\epsilon f}$; we thus consider only autoionization to ϵh. In this approximation we find

$$n^3\Gamma=\begin{cases}1.0\times10^4\ \text{cm}^{-1}, & J=5\\ 1.2\times10^4\ \text{cm}^{-1}, & J=3 .\end{cases} \tag{7}$$

These results are in reasonable agreement with the experimental results.

In sum this rather simple model gives excellent values for the splittings of the $6p_{3/2}ng_k$ states, allowing us to assign the levels, and gives reasonable values for the autoionization rates. This suggests that these states should be an excellent test for a serious calculation.

V. QUANTUM-DEFECT-THEORY TREATMENT

One of the interesting aspects of the Ba $6png$ states is the interaction between the $6p_{jl}ng_k$ channels. By the term channel we mean, for example, the Ba $6p_{1/2}ng_{9/2}$ $J=5$ states and the Ba $6p_{1/2}\epsilon g_{9/2}$ $J=5$ continuum above the Ba^+ $6p_{1/2}$ limit. Above the Ba^+ $6p_{1/2}$ limit the interaction is manifested in the autoionization of the $6p_{3/2}ng_k$ states to the Ba^+ $6p_{1/2}$ state with the ejection of an ϵg electron, and below the $6p_{1/2}$ limit by the interseries interactions leading to perturbations of the spectra. Examples of this are shown in Fig. 5 and 6.

The most straightforward way of relating these phenomena is to use quantum-defect theory. We have used the formulation of Cooke and Cromer,[12] which is similar to an approach used by Giusti-Suzor and Fano.[19] We have chosen to use this formulation primarily because its parameters match more closely our experimental results. Specifically, the parameters are the quantum defects δ_i of each series of autoionizing states and coupling parameters

R'_{ij} to other channels. Thus if we have a two-channel problem in which there is a series of discrete autoionizing states (channel 1) coupled to the continuum (channel 2) two parameters, δ_1 and R'_{12}, completely describe the series of autoionizing states. The quantum defect δ_1 specifies the energy of the discrete state, and the autoionization rate Γ_{12} is given by[12]

$$\Gamma_{12}=\frac{2(R'_{12})^2}{\pi(n^*)^3}\ , \tag{8}$$

where n^* is the effective quantum number of the autoionizing state. The total autoionization rate is given by the sum of the rates to all the allowed continua, as shown by Eq. (5).

For the excitation method we use, which occurs with the outer electron at large orbital radius, this is a particularly convenient form of quantum-defect theory. It is, of course, fundamentally the same as the formulation of Fano,[20] which is more suitable for describing excitation processes in which the excitation takes place with the outer electron at small orbital radius. The essential difference is that the Cooke and Cromer formulation does not specify the phase of the continuum whereas the Fano formulation does. As our experiments are not sensitive to the continuum phase the Cooke and Cromer[13] approach is appropriate.

Specifically, we have analyzed the $6png$ $J=5$ states. The odd-parity $J=5$ channels consist of the three $6png$ channels and eight continuum channels built on the Ba^+ $6s$ and $5d$ states. This is clearly too many channels for a meaningful analysis, and we have assumed that the autoionization of the three $6png$ channels occurs into three linear combinations of these continua represented by three continua, 1, 2, and 3. Thus the quantum-defect-theory model we have used for the $J=5$ states is a six-channel model with the channels given in Table V. The parameters we have used to fit our data are given in Table VI.

The parameters of Table VI fit most of the features of the $6png$ $J=5$ states. Above the Ba^+ $6p_{1/2}$ limit the $6p_{3/2}ng_k$ states have quantum defects of 0.00 and 0.07 and widths of $0.032n^{-3}$, in good agreement with the experimental observations. Below the Ba^+ $6p_{1/2}$ limit the fit yields the parameters given in Tables I and II. In addition, the fit gives the computed spectra of Fig. 8 which correspond to the observed spectra of Figs. 5 and 6. All in all, the quantum-defect-theory fit reproduces satisfactorily many data with few parameters.

TABLE VI. $J=5$ quantum-defect parameters.

$\delta_1=0.015$
$\delta_2=0.070$
$\delta_3=0.000$
$R'_{12}=0.10$
$R'_{13}=0.10$
$R'_{14}=0.22$
$R'_{25}=0.20$
$R'_{36}=0.20$

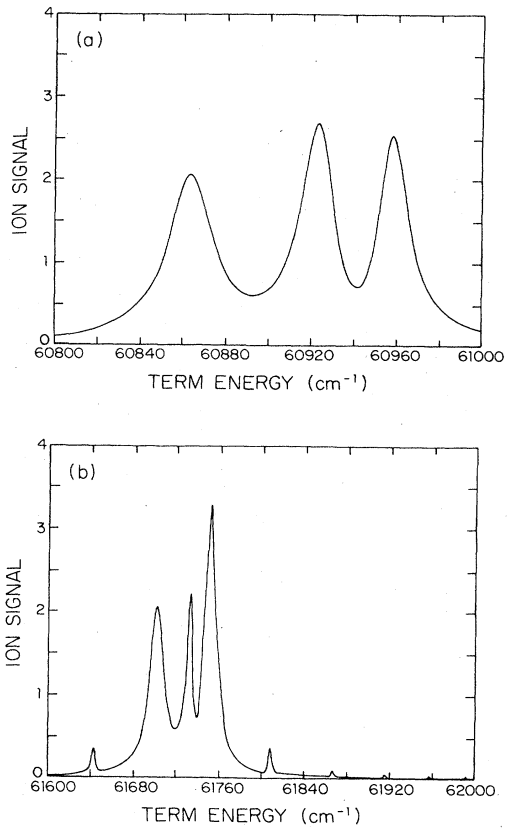

FIG. 8. Calculated spectra of $6sng\ ^1G_4-6p_{3/2}ng_k$ $J=5$ states. (a) $6s6g\ ^1G_4-6p_{3/2}6g_{11/2,9/2}$, note the hole in the center of the $6p_{3/2}6g_{11/2}$ state at 60 940 cm^{-1} which comes from the degenerate $6p_{1/2}6g_{9/2}$ state. This is to be compared to Fig. 5. (b) $6s7g\ ^1G_4-6p_{3/2}7g_{11/2,9/2}$. Note the interferencelike features arising from the interaction with the $6p_{1/2}ng_{9/2}$ states. This is to be compared to Fig. 6.

VI. CONCLUSION

From a practical point of view the importance of these experiments is in verifying that we can calculate many of the properties such as autoionization rates of these high angular momentum states to 50% accuracy using a very simple approach. This suggests that in calculating macroscopic properties such as dielectronic recombination rates which depend on even higher angular momentum states that simple models are adequate.

From a more basic point of view the $6png$ states reported here represent the first study of states which autoionize by means of a long-range Coulomb interaction. It is thus not surprising that the results are in qualitative agreement with relatively simple calculations. On the other hand, it is clear that not all features of the data are in complete accord with the simple model. It should thus be interesting to both observe experimentally the finer details of the autoionization process, such as the branching ratios to final ion and electron states, and to carry out more sophisticated calculations.

ACKNOWLEDGMENTS

It is a pleasure to acknowledge useful discussions with D. L. Huestis and O. C. Mullins. This work has been supported by the U.S. Department of Energy (Office of Basic Energy Sciences).

---

*Present address: Department of Physics, University of Wisconsin, Madison, WI 53706.

†Present address: Fundamenteel Onderzoek der Materie—Instituut voor Atoom- en Molecuulfysica, Kruislaan 4007, NL-1098 SJ Amsterdam, The Netherlands.

‡Present address: Department of Physics, University of Virginia, Charlottesville, VA 22901.

[1]V. L. Jacobs, J. Davis, and P. C. Kepple, Phys. Rev. Lett. **37**, 1370 (1976).

[2]W. E. Cooke, T. F. Gallagher, S. A. Edelstein, and R. M. Hill, Phys. Rev. Lett. **41**, 1648 (1978).

[3]U. Fano, Phys. Rev. **124**, 1866 (1961).

[4]E. U. Conden and G. H. Shortley, *Theory of Atomic Spectra* (Cambridge University, London, 1957).

[5]A. R. Edmonds, *Angular Momentum in Quantum Mechanics* (Princeton University, Princeton, 1960).

[6]O. C. Mullins, R. Chien, J. E. Hunter III, J. S. Keller, and R. S. Berry, Phys. Rev. A **31**, 321 (1985).

[7]F. Gounand, T. F. Gallagher, W. Sandner, K. A. Safinya, and R. Kachru, Phys. Rev. A **27**, 1925 (1983).

[8]T. W. Hansch, Appl. Opt. **11**, 895 (1972).

[9]M. G. Littman and H. J. Metcalf, Appl. Opt. **17**, 2224 (1978).

[10]J. R. Rubbmark, S. A. Borgstrom, and K. Bockasten, J. Phys. B **10**, 421 (1977).

[11]P. Camus, M. Dieulin, and A. El Himdy, Phys. Rev. A **26**, 379 (1982).

[12]W. E. Cooke and C. L. Cromer (unpublished).

[13]W. E. Cooke, S. A. Bhatti, and C. L. Cromer, Opt. Lett. **7**, 69 (1982).

[14]W. E. Cooke and S. A. Bhatti, Phys. Rev. A **26**, 391 (1982).

[15]J. P. Connerade, Proc. Phys. Soc. London, Sect. A **362**, 361 (1978).

[16]J. H. Van Vleck and N. G. Whitelaw, Phys. Rev. **44**, 551 (1933).

[17]H. A. Bethe and E. A. Salpeter, *Quantum Mechanics of One- and Two-Electron Atoms* (Academic, New York, 1957).

[18]A. Lindgard and S. E. Neilsen, At. Data Nucl. Data Tables **19**, 534 (1977).

[19]A. Giusti-Suzor and U. Fano, J. Phys. B **17**, 218 (1984).

[20]U. Fano, Phys. Rev. A **2**, 353 (1970).